# Spontaneous Symmetry Breaking of Achiral Molecules Leading to the Formation of Homochiral Superstructures that Exhibit Mechanoluminescence

Zheng-Fei Liu[†], Xin-Yi Ye[†], Lihua Chen[‡], Li-Ya Niu[†], Wei Jun Jin[†]*, Shaodong Zhang[‡]* and Qing-Zheng Yang[†]*

[†] Key Laboratory of Radiopharmaceuticals, Ministry of Education, College of Chemistry, Beijing Normal University, Beijing 100875, China.

[‡]School of Chemistry and Chemical Engineering, Shanghai Jiao Tong University, 800 Dongchuan Road, Shanghai 200240, China.

*Email: wjjin@bnu.edu.cn, sdzhang@sjtu.edu.cn, qzyang@bnu.edu.cn.

## ABSTRACT

Chirality, with its intrinsic symmetry-breaking feature, is frequently utilized in the creation of acentric crystalline functional materials that exhibit intriguing optoelectronic properties. On the other hand, the development of chiral crystals from achiral molecules offers a solution that bypasses the need for enantiopure motifs, presenting a promising alternative and thereby expanding the possibilities of the self-assembly toolkit. Nevertheless, the rational design of achiral molecules that prefer spontaneous symmetry breaking during crystallization has so far been obscure. In this study, we present a series of six achiral molecules, demonstrating that when these conformationally flexible molecules adopt a *cis*-conformation and engage in multiple non-covalent interactions along a helical path, they collectively self-assemble into chiral superstructures consisting of single-handed supramolecular columns. When these homochiral supramolecular columns align in parallel, they form polar crystals that exhibit intense luminescence upon grinding or scraping. We therefore demonstrate our molecular design strategy could significantly increase the likelihood of symmetry breaking in achiral molecular synthons during self-assembly, offering a facile access to novel chiral crystalline materials with unique optoelectronic properties.

## INTRODUCTION

Symmetry and symmetry breaking are fundamental concepts in various fields, including mathematics, physics, chemistry, and philosophy. Symmetry breaking entails the loss of specific symmetry elements within a system of higher-order symmetry, resulting in the transformation into one of its subgroups with a lower-order symmetry. According to Pierre Curie,[1] symmetry elaborates the laws of nature, while symmetry breaking is what creates the phenomenon. The principle of symmetry breaking plays essential role in our understanding of nature and the phenomena that occur within it,[2–4] which is also widely applied for the search of emergent properties across various scientific disciplines.[5–10] For instance, inversion symmetry breaking in acentric crystalline phase is the cause that generates piezoelectric effect,[11] second harmonic generation (SHG)[12] and bulk photovoltaic effect (BPVE);[13] while symmetry breaking within polar structures gives rise to pyro- and ferroelectric effect.[13–14] These intriguing optoelectronic properties are indispensable for the state-of-the-art applications in the fields of electronics, energy and information technology.

Employing homochiral building blocks has been demonstrated as a prevalent strategy,[15] which breaks the inversion symmetry and leads to acentric superstructures, and can also enable facile access to polar crystalline materials.[14,16] Spontaneous symmetry breaking during self-assembly of achiral building blocks could offer a promising alternative.[17–19] This approach circumvents the prerequisite of enantiopure motifs, therefore expanding the possibilities of the self-assembling toolkit. However, with the exception of some sporadic serendipities,[20–28] the rational design of such achiral synthons imposes a formidable challenge, as it relies on the delicate interplay between molecular symmetry, conformational flexibility, and noncovalent interactions.[29–31]

Given over 60% of noncentrosymmetric crystals (41/65 Sohncke space groups) exhibit screw symmetry, we recently proposed a strategy that favors spontaneous chiral resolution of racemic molecules, which we termed "*go with the flow*":[18] When rational molecular design facilitates the exerting of multivalent intermolecular interactions along the helical trajectory of screw symmetry of the molecular packing, the racemates could experience narcissistic self-sorting during crystallization, leading to the formation of homochiral conglomerates. We also applied this strategy to a series of achiral D-A molecules.[17] As their chiral conformations were clamped by multivalent noncovalent interactions, which facilitate the packing of the molecules along the supramolecular $2_1$-helices, leading to the formation of chiral crystals. While this symmetry breaking strategy is promising, the generality is yet to be confirmed.

In this report, we designed a library of six achiral pyrene-containing molecules and two counterexamples to demonstrate the powerful strategy for spontaneous symmetry breaking. We demonstrate, when the molecules adopt a *cis*-conformation and allow to exert multiple interactions along the helical trajectory of screw symmetry within the crystalline phase, that the symmetry of the flexible molecules can be broken during self-assembly, leading to the formation of chiral crystals, which are noncentrosymmetric (Figure 1). Among six chiral crystals, three of them are polar and three nonpolar. When the polarity of the crystals resulting from symmetry breaking is coupled with the intrinsic photophysical property of pyrene moieties, the three polar crystals exhibit intense luminescence upon scraping or grinding, known as mechanoluminescence (ML) or triboluminescence phenomenon, which has recently showed promise in the applications of sensing, display, optogenetics and so on.[32–37] On the other hand, the three nonpolar chiral crystals don't exhibit any ML behavior. This comparison therefore reveals that the polarity, rather than the noncentrosymmetric

structure of a luminescent crystal, could be used as a design principle for the search of novel ML materials (Figure 1).

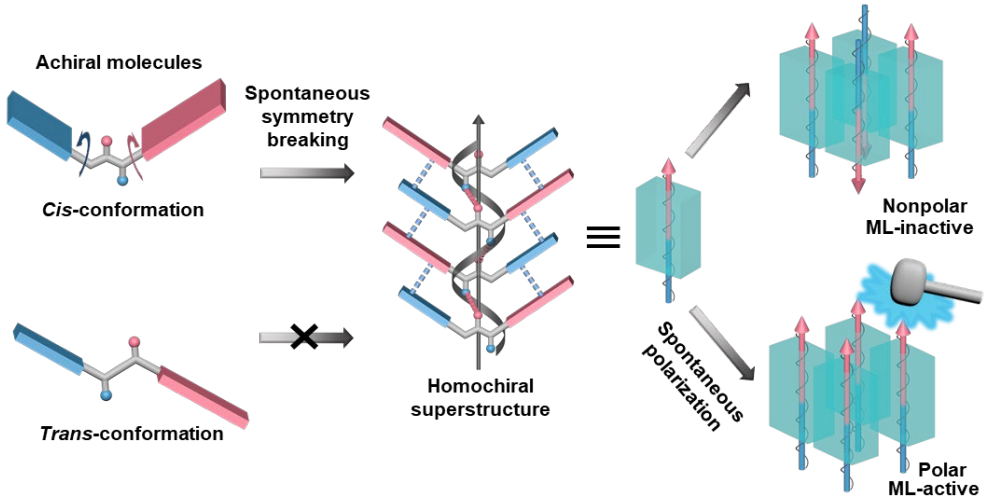


**Figure 1**. Schematic illustration of chiral and polar symmetry breaking during the self-assembly of achiral molecular with *cis*-conformation rather than *trans*-conformation. The formation of chiral crystals of achiral molecules is facilitated by multiple interactions exerting along the trajectory of the screw symmetry of the crystal. The parallel alignment of homochiral columns results in polar superstructures that exhibit mechanoluminescence behavior, while their antiparallel alignment of these homochiral columns are silent in mechanoluminescence.

## RESULT AND DISCUSSION

**Molecular design of achiral molecules that self-assemble into chiral crystals.** We first designed an achiral molecule perfluorophenyl 4-(pyren-1-yl)butanoate (**FPy**), which consists of perfluorophenyl, pyrenyl and a flexible linker (Figure 2a). The syntheses, chemical characterizations by $^{1}$H and $^{13}$C nuclear magnetic resonance (NMR), and electrospray ionization mass spectroscopy (ESI-MS) are given in the Supporting Information. The perfluorophenyl and pyrenyl groups of **FPy** are connected by an ester containing linker, which confers the conformational flexibility of the molecule. By density functional theory (DFT) calculations, we first investigated the minimum-energy isomerization with the rotation of perfluorophenyl ($\theta_1$) and pyrenyl ($\theta_2$) groups (Figure 2b). The most stable conformations of **FPy** were observed when the $\theta_1$ and $\theta_2$ are around ±90°. This result suggests that **FPy** has a potential chiral

conformation (*P*- or *M*-**FPy**) and the alkyl chain containing carbonyl group tends to be perpendicular to the perfluorophenyl and pyrenyl planes (Figure 2b). The relatively low rotation energy barriers of the perfluorophenyl (7.8 kcal·mol$^{-1}$) and pyrenyl (1.9 kcal·mol$^{-1}$) groups confirm the achiral nature of **FPy** in solution, as their conformations average out due to the ultrafast intramolecular motion.

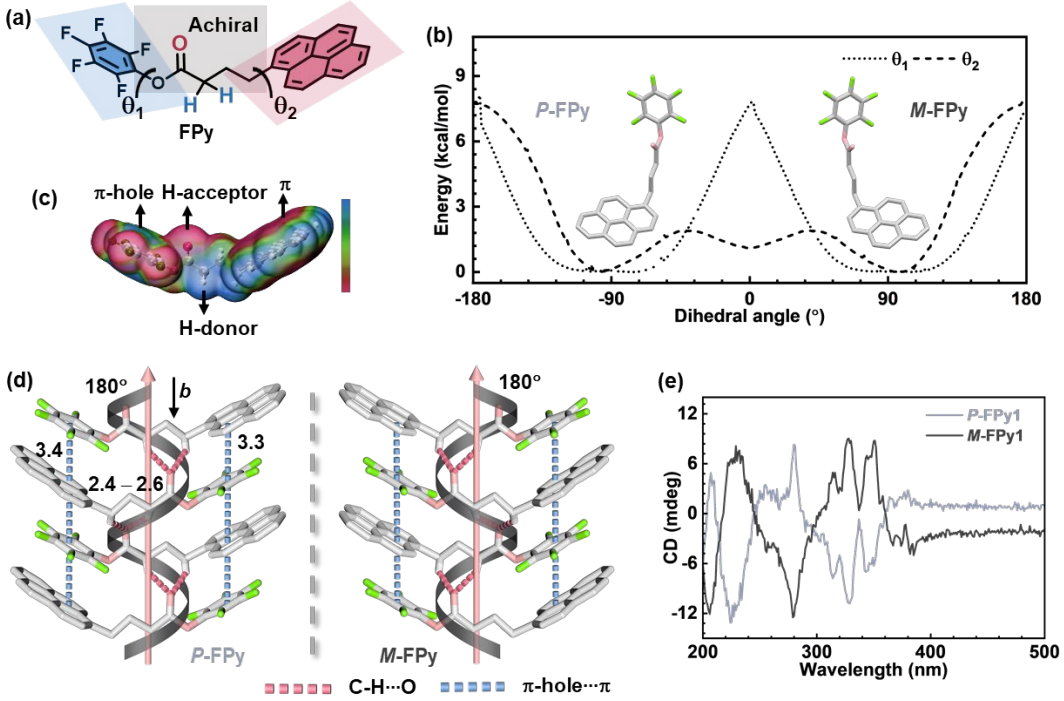


**Figure 2**. (a) Molecular structure of **FPy**. (b) Potential energy landscape along the rotation of the pentafluorophenyl and pyrenyl groups of **FPy**. (c) Molecular surface electrostatic potential (SEP) mapping of **FPy**. The scale of SEP mapping from +15 kcal/mol to –15 kcal/mol, represented with colour change from blue to red. (d) Molecular packing within the homochiral helical columns of *P*-**FPy** and *M*-**FPy** in crystals, respectively. The pink arrows indicate their polarization directions. (e) Solid-state CD spectra of individual bulk *P*-**FPy** and *M*-**FPy** crystals dispersed in KBr tablet, respectively.

The perfluorophenyl and pyrenyl groups of **FPy** can function as donor and accepter of π-hole interaction,[38] respectively, which serve as effective driving force for molecular stacking. Additionally, the carbonyl and methylene groups can act as acceptor and donor of hydrogen bond (H-bond),[39–41] respectively, forming H-bond perpendicular to the perfluorophenyl and pyrenyl planes. The molecular surface electrostatic potential (SEP) mapping of **FPy** confirms the sites and directionality of

these noncovalent interactions (Figure 2c). The donors of the π-hole interaction and H-bond are situated in positive potential regions (shown in blue), while the acceptors are found in negative potential regions (in red).

We then investigated their absolute conformation using single crystal X-ray diffraction (SC-XRD). By slow evaporation of the dichloromethane/*n*-hexane (2/1, v/v) solution of **FPy**, it crystallized into monoclinic space group $P2_1$ (Figure 2d, Table S1 and S2), which belongs to chiral polar point group 2 ($C_2$). Intriguingly, each crystal is solely composed of **FPy** molecules in either *P*- or *M*-conformation. The results confirm the spontaneous symmetry breaking during the crystallization of these otherwise achiral molecules.

The detailed analysis of these crystal structures provides compelling evidence for the underlying driving force behind this symmetry breaking (Figure 2d). Each homochiral conglomerate is composed of supramolecular helical columns of single handedness. The formation of these helical columns is facilitated by the helical network of C-H···O H-bonds (2.4–2.6 Å, red dashed lines) between carbonyl and methylene groups on the flexible linker, which are stabilized by π-hole···π interactions (3.3–3.4 Å, cyan dashed lines) between perfluorophenyl and pyrenyl moieties. The π-hole···π interactions act as "clamps", facilitating the formation of helical column by connecting the **FPy** molecules.

In addition, the perfluorophenyl and pyrenyl motifs of each **FPy** molecule are located on the same side of the flexible linker, adopting a chiral *cis*-conformation. Around the crystallographic *b*-axis, each **FPy** molecule rotates by 180° with respect to another, so that they are packed in a head-to-tail manner along the helical trajectory, forming a chiral supramolecular $2_1$-helix, in line with our previously proposed strategy

of "go with the flow".[18] The helices are extended on the *ac* plane to afford the chiral polar monoclinic crystalline phase (Figure S9).

The chirality of *P*- and *M*-**FPy** conglomerates was further confirmed by circular dichroism (CD) spectroscopy in solid state, with the previously analysed crystals by SC-XRD dispersed in KBr (Figure 2e). The CD spectra show that *P*- and *M*-crystals exhibit mirror-image profile in the region of UV–Vis absorbance (Figure S19). Taking the *P*-crystal for instance, it displays a positive cotton effect at 380 nm, followed by a negative one at 347 nm. The characteristic positive-to-negative bisignate curve confirms the *P*-configuration of the crystal.

The prerequisite of H-bonding was verified with a reference compound, 1-(4-(perfluorophenoxy)butyl)pyrene (**FOPy**), which is deprived of the carbonyl group as compared to **FPy** molecule (Figure S10). Under the same conditions **FOPy** molecules crystallized into centrosymmetric space group $P2_1/c$ (Table S3). When the carbonyl group is replaced by a methylene in **FOPy**, the octuple C-H···π interactions with an antiparallel orientation (2.6–2.7 Å) between alkyl chain and pyrene become the primary driving forces for the molecular stacking (Figure S10), consequently leading to the formation of centrosymmetric crystals that are achiral.

We further investigated the impact of molecular conformation on their packing during self-assembly, with the comparison of perfluorophenyl 3-(pyren-1-yl)propanoate (**FPy1**) and **FPy** (Figure 3a). **FPy1** has one less methylene in its alkyl chain as compared to **FPy**, while the SEP mapping of **FPy1** (Figure 3a) confirms that its sites of π-hole···π interaction and H-bond remain the same as in **FPy** molecule (Figure 2c). The SC-XRD analysis reveals that **FPy1** molecules adopts a *trans*-conformation, *i.e.*, its perfluorophenyl and pyrenyl motifs are located on the different sides of the flexible linker. Within the crystalline phase, every two **FPy1** molecules of

mirror image are packed in the opposite orientation (Figure 3b), leading to the formation of achiral crystals that belong to *C*2/*c* centrosymmetric space group (Table S4). In addition, two-fold H-bonds are aligned in antiparallel within every **FPy1** dimer (Figure 3b and 3c), which is in contrast to the helical H-bond network formed in the homochiral columns formed by **FPy**.

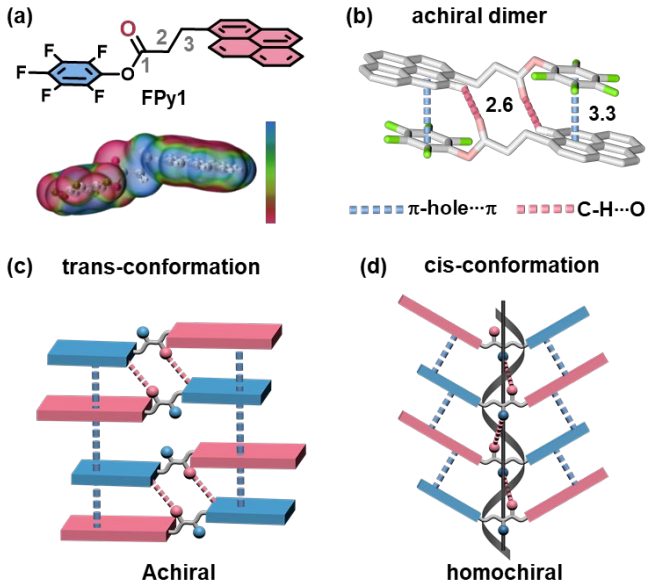


**Figure 3**. (a) The molecular structure and SEP mapping of **FPy1**. The scale of SEP mapping from +15 kcal/mol to –15 kcal/mol, represented with colour change from blue to red. (b) An achiral dimer of **FPy1** with *trans*-conformation in the crystalline phase. The C-H···O hydrogen bonds and π-hole···π interactions are shown in red and cyan dashed lines, respectively. (c) The simplified model represents the centrosymmetric stacking of achiral molecules with *trans*-conformation. (d) The simplified model represents the homochiral stacking of achiral molecules with *cis*-conformation.

This result emphasizes that, in addition to directional noncovalent interactions, molecular conformation plays a significant role in molecular packing. The *cis*-conformation is more susceptible to facilitate symmetry breaking than the *trans*-conformation does, as illustrated with the comparison of simplified stacking models depicted in Figures 3c and 3d.

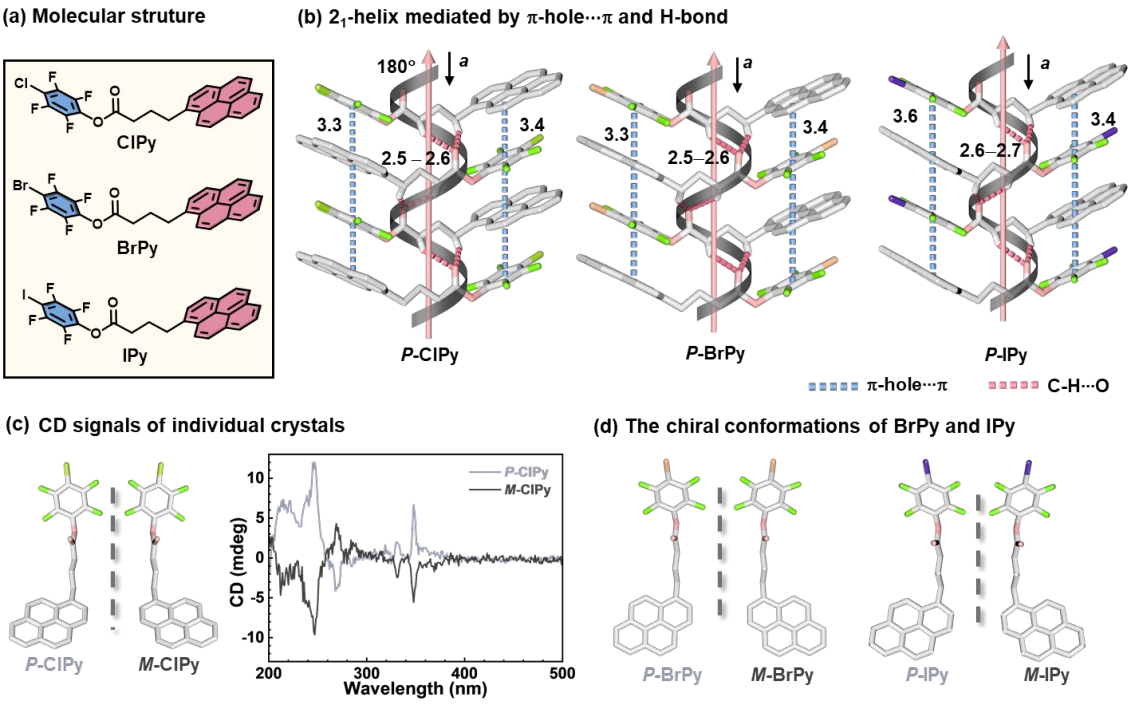


**Figure 4**. (a) Molecular structures of **ClPy**, **BrPy** and **IPy**. (b) The $2_1$-helices of self-assembled by **ClPy**, **BrPy** and **IPy** molecules, mediated by π-hole···π interactions and C-H···O H-bonds. The pink arrows indicate the polarization directions of their respective $2_1$-helices. (c) The chiral conformations in *P*-**ClPy** and *M*-**ClPy** crystals, respectively (left). Solid-state CD spectra of individual bulk *P*-**ClPy** and *M*-**ClPy** crystals dispersed in KBr tablets, respectively (right). (d) The chiral conformations in *P*-**ClPy**, *M*-**ClPy** (left) and *P*-**IPy**, *M*-**IPy** (right) crystals, respectively. The hydrogen atoms not involved in hydrogen bonding are omitted for clarity.

**Generality of rational design of achiral molecules for symmetry breaking during self-assembly to form chiral crystalline phase.** To validate the reliability of our design principle of "*go with the flow*", we synthesized three analogues, *i.e.*, 4-chloro-2,3,5,6-tetrafluorophenyl 4-(pyren-1-yl)butanoate (**ClPy**), 4-bromo-2,3,5,6-tetrafluorophenyl 4-(pyren-1-yl)butanoate (**BrPy**) and 2,3,5,6-tetrafluoro-4-iodophenyl 4-(pyren-1-yl)butanoate (**IPy**), which replace the fluorine atom at the *para*-position of **FPy** with chlorine, bromine, or iodine atoms, respectively (Figure 4a). The SEP mapping of three compounds reveals that the interaction sites of π-hole···π interaction and C-H···O H-bond are retained (Figure S17). Besides, these halogen atoms X (X = Cl/Br/I) provide distinct positive potential regions (σ-hole), which would allow the formation of halogen bonds with the nucleophilic regions of neighboring molecules.[38,42] Under the same condition of crystallization, all three molecules experienced

spontaneous symmetry breaking, leading to the formation of chiral crystals composed of molecules with homochiral conformation. The SC-XRD analysis reveals that all three molecules adopt *cis*-conformation, and self-assemble into orthorhombic space group $P2_12_12_1$ for **ClPy** and **BrPy**, and tetragonal $P4_12_12$/$P4_32_12$ for **IPy**, which belong to chiral nonpolar point group 222 ($D_2$) and 422 ($D_4$), respectively (Table S5–S10).

The three molecules exhibit nearly identical *cis*-conformations, and their supramolecular $2_1$-helices are driven by π-hole···π interactions and C-H···O H-bonds, reminiscent of **FPy** (Figure 4b). As for **ClPy** and **BrPy**, it is worth noting that the chlorine and bromine atoms indeed form halogen bonds, *i.e.*, C-Cl···F (3.2 Å) and C-Br···F (3.1 Å), with the molecules of the adjacent supramolecular helices, which induces the up-side down packing of one $2_1$-helix with the neighboring helices. These homochiral supramolecular helices self-organize in an antiparallel fashion, therefore forming a chiral nonpolar crystalline phase (Figure S11 and S12). This result is in contrast with the polar crystals formed by **FPy**, within which the homochiral supramolecular helices are aligned in parallel, so that their dipoles are accumulated. (Figure S9). As for **IPy**, C-I···π (3.6 Å) halogen bonds induce $2_1$-helices to further assemble into nonpolar $4_1$/$4_3$-helices via the operation of $4_1$/$4_3$-screw symmetry (Figure S13). The $4_1$/$4_3$-helices eventually form a chiral nonpolar crystalline. The chirality of **ClPy** and **IPy** crystals was also confirmed by CD in solid state (Figure 4c and Figure S18). **BrPy** molecules crystallized into needle-like crystals that are too small to measure solid-state CD of an individual crystal.

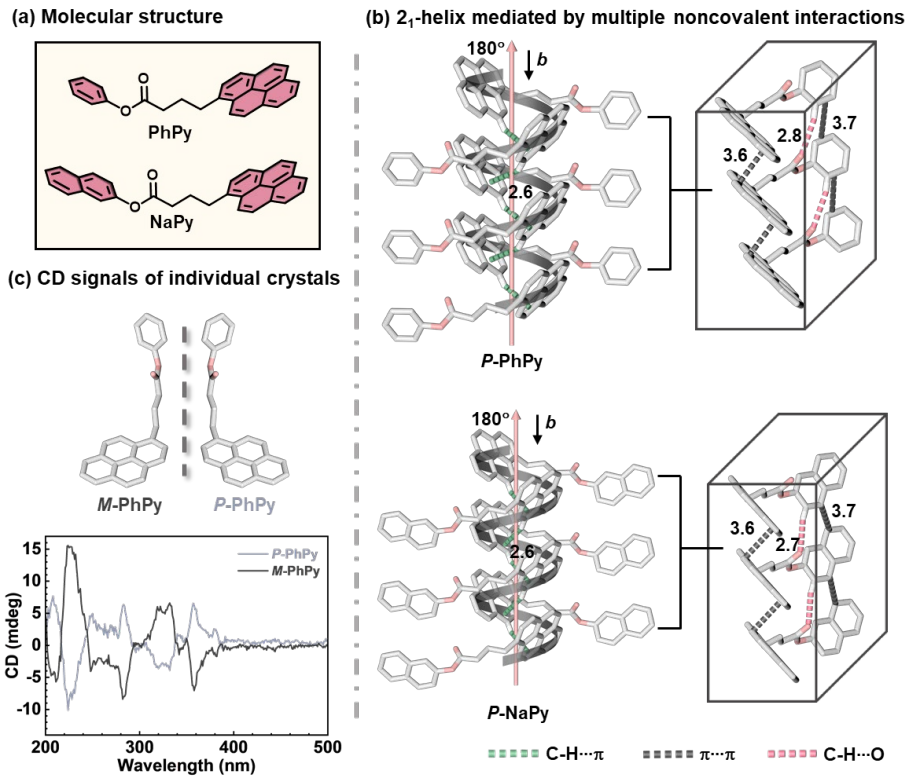


**Figure 5**. (a) The molecular structures of achiral molecules **PhPy** and **NaPy** that undergo chiral symmetry breaking. (b) The $2_1$-helices of self-assembled by **PhPy** (top) and **NaPy** (below) molecules, mediated by multiple noncovalent interactions including C-H···π, π···π and C-H···O interactions along the screw symmetry. (c) The chiral conformations in *M*-**PhPy** and *P*-**PhPy** crystals, respectively (top). Solid-state CD spectra of individual bulk *M*-**PhPy** and *P*-**PhPy** crystals dispersed in KBr tablet, respectively (below).

We also synthesized phenyl 4-(pyren-1-yl)butanoate (**PhPy**) and naphthalen-2-yl 4-(pyren-1-yl)butanoate (**NaPy**), which replace the perfluorophenyl group of **FPy** with phenyl and naphthyl groups, respectively (Figure 5a). Under the same condition of crystallization, both **PhPy** and **NaPy** self-assembled into monoclinic space group $P2_1$, belonging to chiral polar point group 2 ($C_2$, Table S11–S14). The two molecules exhibit nearly identical arrangements in chiral polar crystalline phases (Figure 5b, S14 and S16).

To avoid verbiage, only the conglomerate of *M*-**PhPy** is illustrated here for example, the molecules also exhibiting *cis*-conformation. These molecules are arranged off crystallographic *b*-axis. Each molecule rotates by 180° with respect to another (Figure 5b). As a result, it forms a polar supramolecular $2_1$-helix, which is mediated by multiple noncovalent interactions along the screw symmetry, including C-H···π (2.6 Å),

π···π interactions (3.7–3.6 Å) and C-H···O (2.8 Å) H-bonds. Each supramolecular helix consists of two columns located on the opposite side of *b*-axis. These helical columns are connected by C-H···π interactions. In each column, the π···π interactions act as conformation clamps between **PhPy** molecules (Figure 5b). Ultimately, the polar supramolecular helices are extended parallelly on the *ac* plane to afford the chiral polar monoclinic crystalline phase (Figure S14). The chirality of **PhPy** bulky crystals was also confirmed by CD in solid state (Figure 5c).

**Mechanoluminescence activity of these pyrene-based crystals.** Despite the first observation of the ML phenomenon since 1605 by Francis Bacon,[43] no consensus on its mechanism and rational design principle has merged.[37, 44–46] Different factors, including molecular structure,[47–48] intermolecular interactions,[36] molecular packing[49], and impurity[50–51] are thought to play significant role in generating this appealing phenomenon. It's therefore important to note that, because of the simultaneous presence of various factors that contribute to the ML process, a careful elaboration of its mechanisms has yet to establish.

According to Zink and coworkers,[44] noncentrosymmetric, polar crystalline structures are necessary for the occurrence of ML, which is however contradicted with observation of ML from centrosymmetric, nonpolar structures made by Sweeting et al.[45] With six chiral, i.e., noncentrosymmetric crystals in hand, we therefore would like to present a plausible correlation between the ML process and the polarity of the crystals.

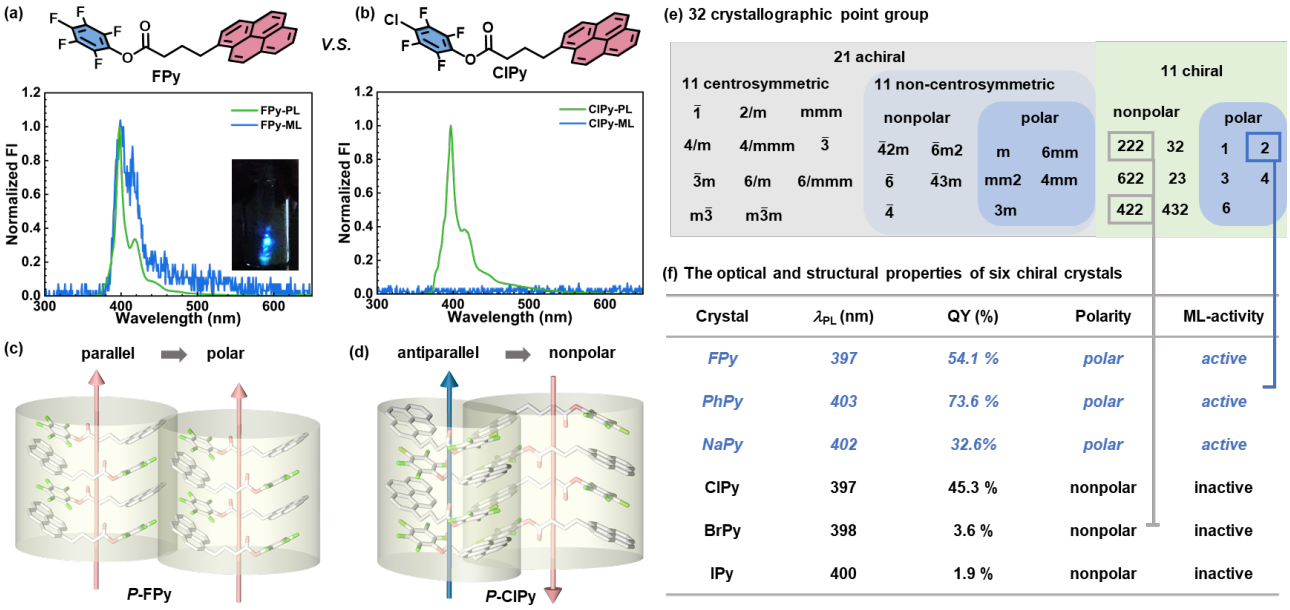


| Crystal | $\lambda_{PL}$ (nm) | QY (%) | Polarity | ML-activity |
|---|---|---|---|---|
| *FPy* | *397* | *54.1 %* | *polar* | *active* |
| *PhPy* | *403* | *73.6 %* | *polar* | *active* |
| *NaPy* | *402* | *32.6%* | *polar* | *active* |
| ClPy | 397 | 45.3 % | nonpolar | inactive |
| BrPy | 398 | 3.6 % | nonpolar | inactive |
| IPy | 400 | 1.9 % | nonpolar | inactive |

**Figure 6**. The photoluminescence and mechanoluminescence spectra of (a) **FPy** and (b) **ClPy** crystals, respectively. Inset in (a): an image presenting mechanoluminescence of **FPy** crystals upon scraping with a glass rod. (c) Two supramolecular homochiral helical columns of **FPy** alignment in parallel orientation. Pink arrows indicate the alignments of dipoles of columns. (d) Two supramolecular homochiral helical columns of **ClPy** alignment in antiparallel orientation. Blue and pink arrows indicate the cancellation of dipoles of two columns. (e) The 32 crystallographic point groups, within which 11 groups are chiral. (f) The comparison of photophysical properties, polarity and ML-activity of six chiral crystals presented in our study.

The photophysical properties of these six pyrene-based derivatives in solution and crystal state were fully characterized (Figure 6). These compounds exhibit similar absorption and fluorescence behaviors in solution, all originating from the pyrene chromophore (Figure S23). It is worth noting that, as a classical type of polycyclic aromatic hydrocarbons, pyrene typically display excimer emission accompanied by concentration quenching in aggregated state. However, in the solid state, the photoluminescence (PL) of the six compounds exhibits monomeric emission from pyrene, with an emission peak at around 400 nm (Figure 6a and S24). We speculate that, as there is no direct contact between pyrene moieties in their crystalline phases (Figures 2d, 4b and 5b), this particular molecular packing might prevent the formation of excimers in the excited state and effectively overcome the aggregation-caused quenching, leading to the bright blue fluorescence of **FPy**/**ClPy**/**PhPy**/**NaPy** with the

high solid-state fluorescence quantum yield of 54.1%, 45.3%, 73.6% and 32.6%, respectively. On the other hand, as the heavy atom effect of bromine and iodine atoms leads to fluorescence quenching, only low fluorescence quantum yields of **BrPy** (3.6%) and **IPy** (1.9%) was observed in solid state.

The ML behaviors of these compounds were then investigated. Upon scraping or grinding the crystalline powders, **FPy**, **PhPy** and **NaPy** belonging to polar point group 2 ($C_2$) exhibit a bright blue ML emission (Figure 6b and S25), whereas **ClPy**, **BrPy** and **IPy** belonging to nonpolar point group 222 ($D_2$) and 422 ($D_4$) are ML-silent (Figure 6e and 6f). The ML spectra of **FPy**, **PhPy** and **NaPy** are similar to their PL spectra, which indicates that their ML is attributed to the intrinsic monomeric emission of pyrene, which rather excludes the possible $N_2$ emission caused by dielectric breakdown.[52] These results therefore suggest that the polarity of crystals is a key factor for ML-activity.

Furthermore, a comprehensive comparison of the structural and optical properties between **FPy** and **ClPy** further highlights the structure-property correlation. **FPy** and **ClPy** share almost identical structural parameters that affect their optical properties in crystalline state, including molecular structures, molecular conformations, stacking patterns in supramolecular helical columns and intermolecular interactions (Figure 2d and 3b). Consequently, both **FPy** and **ClPy** exhibit similar photophysical properties in crystalline state, with their fluorescent peak profiles and wavelengths being virtually indistinguishable (Figure 6a and 6b). Additionally, the fluorescent intensity decay of **FPy** and **ClPy** follows a single exponential pattern, with similar lifetimes of 131.0 ns and 106.2 ns, respectively (Figure S26). Their solid-state quantum yields are also similar. The notable difference between **FPy** and **ClPy** crystals can only be attributed to the orientation of their supramolecular helical columns. **FPy** helical columns adopt

a parallel arrangement, leading to the spontaneous polarization in crystalline phase, while **ClPy** helical columns adopt an antiparallel arrangement, resulting in cancellation of their dipoles (Figure 6c and 6d). This strict comparison of their structural and optical properties clearly unravels that the polarity of the crystal is the pivotal factor for the ML activity.

## CONCLUSION

In summary, we designed a series of six achiral pyrene-based molecules with conformational flexibility. When the molecules adopt a *cis*-conformation and allow to exert multiple interactions along the helical trajectory of screw symmetry within the crystalline phase, these otherwise achiral molecules experience spontaneous symmetry breaking during crystallization, resulting into the formation of chiral superstructures. Out of the six chiral crystals, three polar crystals exhibit mechanoluminescence while the other three nonpolar crystals are ML-silent. Our work therefore presents a plausible correlation between the ML process and the polarity of the crystals. We believe that this work may inspire a deeper understanding and exploration of symmetry breaking during the self-assembly of achiral supramolecular building blocks, which can be applied for the search of the emergent functions of the resulting superstructures in the future.

## ASSOCIATED CONTENT

### Supporting Information

The Supporting Information is available free of charge on the ACS Publications website. Crystallographic data have been deposited with the Cambridge Crystallographic Data Centre as entries CCDC 2296668, 2296663, 2296672, 2296675, 2296754, 2296677, 2296679, 2064841, 2296688, 2296681, 2296690, 2296692, 2296695 and 2296700. Materials and characterization methods, experimental and theoretical calculation details, crystal structures and compound characterization.

Crystal structure for *M*-**FPy** (CIF)

Crystal structure for *P*-**FPy** (CIF)

Crystal structure for **FOPy** (CIF)

Crystal structure for **FPy1** (CIF)

Crystal structure for *M*-**ClPy** (CIF)

Crystal structure for *P*-**ClPy** (CIF)

Crystal structure for *M*-**BrPy** (CIF)

Crystal structure for P-**BrPy** (CIF)

Crystal structure for *M*-**IPy** (CIF)

Crystal structure for *P*-**IPy** (CIF)

Crystal structure for *M*-**PhPy** (CIF)

Crystal structure for *P*-**PhPy** (CIF)

Crystal structure for *M*-**NaPy** (CIF)

Crystal structure for *P*-**NaPy** (CIF)

## AUTHOR INFORMATION


### Corresponding Author

**Wei Jun Jin -** *Key Laboratory of Radiopharmaceuticals, Ministry of Education, College of Chemistry, Beijing Normal University, Beijing 100875, P. R. China;* orcid.org/0000-0002-4796-5390; Email: wjjin@bnu.edu.cn

**Shaodong Zhang -** *School of Chemistry and Chemical Engineering, Shanghai Jiao Tong University, 800 Dongchuan Road, Shanghai 200240, China*; orcid.org/0000-0001-7923-8457; Email: sdzhang@sjtu.edu.cn

**Qing-Zheng Yang -** *Key Laboratory of Radiopharmaceuticals, Ministry of Education, College of Chemistry, Beijing Normal University, Beijing 100875, P. R. China;* orcid.org/0000-0002-9131-4907; Email: qzyang@bnu.edu.cn

### Authors

**Zheng-Fei Liu -** *Key Laboratory of Radiopharmaceuticals, Ministry of Education, College of Chemistry, Beijing Normal University, Beijing 100875, P. R. China;* orcid.org/0000-0002-0056-1567

**Xin-Yi Ye -** *Key Laboratory of Radiopharmaceuticals, Ministry of Education, College of Chemistry, Beijing Normal University, Beijing 100875, P. R. China;* orcid.org/0009-0008-2967-3811

**Lihua Chen -** *School of Chemistry and Chemical Engineering, Shanghai Jiao Tong University, 800 Dongchuan Road, Shanghai 200240, China*; orcid.org/0000-0002-6204-9497

**Li-Ya Niu -** *Key Laboratory of Radiopharmaceuticals, Ministry of Education, College of Chemistry, Beijing Normal University, Beijing 100875, P. R. China;* orcid.org/0000-0002-5376-6902

**Notes**

The authors declare no competing interests.

## ACKNOWLEDGMENTS

The authors gratefully acknowledge financial support from National Natural Science Foundation of China (22231001 for Q.-Z.Y., T2325017 and 22271187 for S.Z. and 21974011 for W.J.J.) and Science and Technology Commission of Shanghai Municipality (21JC1401700) for S.Z.

## REFERENCES

1. Curie, P., Sur la symétrie dans les phénomènes physiques, symétrie d'un champ électrique et d'un champ magnétique. *J. Phys. Theor. Appl.* **1894**, *3*, 393–415.
2. Watson, J. D.; Crick, F. H. C., Molecular structure of nucleic acids: A structure for deoxyribose nucleic acid. *Nature* **1953**, *171*, 737–738.
3. Harrison, B. D.; Wilson, T. M. A.; Klug, A., The tobacco mosaic virus particle: structure and assembly. *Philos. Trans. R. Soc. Lond. B Biol. Sci.* **1999**, *354*, 531–535.
4. Blackmond, D. G., The origin of biological homochirality. *Cold Spring Harb. Perspect. Biol.* **2010**, *2*, a002147.
5. Grinenko, V.; Sarkar, R.; Kihou, K.; Lee, C. H.; Morozov, I.; Aswartham, S.; Büchner, B.; Chekhonin, P.; Skrotzki, W.; Nenkov, K.; Hühne, R.; Nielsch, K.; Drechsler, S. L.; Vadimov, V. L.; Silaev, M. A.; Volkov, P. A.; Eremin, I.; Luetkens, H.; Klauss, H. H., Superconductivity with broken time-reversal symmetry inside a superconducting *s*-wave state. *Nat. Phys.* **2020**, *16*, 789–794.
6. Li, X.; Gao, P.; Lai, Y.-Y.; Bazak, J. D.; Hollas, A.; Lin, H.-Y.; Murugesan, V.; Zhang, S.; Cheng, C.-F.; Tung, W.-Y.; Lai, Y.-T.; Feng, R.; Wang, J.; Wang, C.-L.; Wang, W.; Zhu, Y., Symmetry-breaking design of an organic iron complex catholyte for a long cyclability aqueous organic redox flow battery. *Nat. Energy* **2021**, *6*, 873–881.
7. Lin, C.; Kim, T.; Schultz, J. D.; Young, R. M.; Wasielewski, M. R., Accelerating symmetry-breaking charge separation in a perylenediimide trimer through a vibronically coherent dimer intermediate. *Nat. Chem.* **2022**, *14*, 786–793.
8. Mielke, C.; Das, D.; Yin, J. X.; Liu, H.; Gupta, R.; Jiang, Y. X.; Medarde, M.; Wu, X.; Lei, H. C.; Chang, J.; Dai, P.; Si, Q.; Miao, H.; Thomale, R.; Neupert, T.; Shi, Y.; Khasanov, R.; Hasan, M. Z.; Luetkens, H.; Guguchia, Z., Time-reversal symmetry-breaking charge order in a kagome superconductor. *Nature* **2022**, *602*, 245–250.
9. Liu, L. R.; Rosenberg, D.; Changala, P. B.; Crowley, P. J. D.; Nesbitt, D. J.; Yao, N. Y.; Tscherbul, T. V.; Ye, J., Ergodicity breaking in rapidly rotating $C_{60}$ fullerenes. *Science* **2023**, *381*, 778–783.
10. Ok, K. M.; Chi, E. O.; Halasyamani, P. S., Bulk characterization methods for non-centrosymmetric materials: second-harmonic generation, piezoelectricity, pyroelectricity, and ferroelectricity. *Chem. Soc. Rev.* **2006**, *35*, 710–717.
11. Pan, C.; Zhai, J.; Wang, Z. L., Piezotronics and piezo-phototronics of third generation semiconductor nanowires. *Chem. Rev.* **2019**, *119*, 9303–9359.
12. Ding, F.; Griffith, K. J.; Zhang, W.; Cui, S.; Zhang, C.; Wang, Y.; Kamp, K.; Yu, H.; Halasyamani, P. S.; Yang, Z.; Pan, S.; Poeppelmeier, K. R., $NaRb_6(B_4O_5(OH)_4)_3(BO_2)$ featuring noncentrosymmetry, chirality, and the linear anionic group $BO_2^-$. *J. Am. Chem. Soc.* **2023**, *145*, 4928–4933.

13. Yang, M.-M.; Kim, D. J.; Alexe, M., Flexo-photovoltaic effect. *Science* **2018**, *360*, 904–907.
14. Shi, P.-P.; Tang, Y.-Y.; Li, P.-F.; Liao, W.-Q.; Wang, Z.-X.; Ye, Q.; Xiong, R.-G., Symmetry breaking in molecular ferroelectrics. *Chem. Soc. Rev.* **2016**, *45*, 3811–3827.
15. Müller, U., Symmetry relationships between crystal structures: applications of crystallographic group theory in crystal chemistry. Oxford University Press: 2013.
16. Li, P.-F.; Liao, W.-Q.; Tang, Y.-Y.; Qiao, W.; Zhao, D.; Ai, Y.; Yao, Y.-F.; Xiong, R.-G., Organic enantiomeric high-$T_c$ ferroelectrics. *Proc. Natl. Acad. Sci. U. S. A.* **2019**, *116*, 5878–5885.
17. Liu, Z.-F.; Ren, J.; Li, P.; Niu, L.-Y.; Liao, Q.; Zhang, S.; Yang, Q.-Z., Circularly polarized laser emission from homochiral superstructures based on achiral molecules with conformal flexibility. *Angew. Chem. Int. Ed.* **2023**, *62*, e202214211.
18. Zuo, Y.; Liu, X.; Fu, E.; Zhang, S., A pair of interconverting cages formed from achiral precursors spontaneously resolve into homochiral conformers. *Angew. Chem. Int. Ed.* **2023**, *62*, e202217225.
19. Shen, Z.; Jiang, Y.; Wang, T.; Liu, M., Symmetry breaking in the supramolecular gels of an achiral gelator exclusively driven by π–π stacking. *J. Am. Chem. Soc.* **2015**, *137*, 16109–16115.
20. Pincock, R. E.; Perkins, R. R.; Ma, A. S.; Wilson, K. R., Probability distribution of enantiomorphous forms in spontaneous generation of optically active substances. *Science* **1971**, *174*, 1018–1020.
21. Azumaya, I.; Uchida, D.; Kato, T.; Yokoyama, A.; Tanatani, A.; Takayanagi, H.; Yokozawa, T., Absolute helical arrangement of stacked benzene rings: heterogeneous double-helical interaction comprising a hydrogen-bonding belt and an offset parallel aromatic–aromatic-interaction array. *Angew. Chem. Int. Ed.* **2004**, *43*, 1360–1363.
22. Tanaka, A.; Inoue, K.; Hisaki, I.; Tohnai, N.; Miyata, M.; Matsumoto, A., Supramolecular chirality in layered crystals of achiral ammonium salts and fatty acids: a hierarchical interpretation. *Angew. Chem. Int. Ed.* **2006**, *45*, 4142–4145.
23. Ohta, E.; Sato, H.; Ando, S.; Kosaka, A.; Fukushima, T.; Hashizume, D.; Yamasaki, M.; Hasegawa, K.; Muraoka, A.; Ushiyama, H.; Yamashita, K.; Aida, T., Redox-responsive molecular helices with highly condensed π-clouds. *Nat. Chem.* **2011**, *3*, 68–73.
24. Ng, C.-F.; Chow, H.-F.; Mak, T. C. W., Halogen-bond-mediated assembly of a single-component supramolecular triangle and an enantiomeric pair of double helices from 2-(iodoethynyl)pyridine derivatives. *Angew. Chem. Int. Ed.* **2018**, *57*, 4986–4990.
25. Wang, F.; Gan, F.; Shen, C.; Qiu, H., Amplifiable symmetry breaking in aggregates of vibrating helical molecules. *J. Am. Chem. Soc.* **2020**, *142*, 16167–16172.
26. Cao, Y.; Alaasar, M.; Zhang, L.; Zhu, C.; Tschierske, C.; Liu, F., Supramolecular meso-trick: ambidextrous mirror symmetry breaking in a liquid crystalline network with tetragonal symmetry. *J. Am. Chem. Soc.* **2022**, *144*, 6936–6945.
27. Stals, P. J. M.; Korevaar, P. A.; Gillissen, M. A. J.; de Greef, T. F. A.; Fitié, C. F. C.; Sijbesma, R. P.; Palmans, A. R. A.; Meijer, E. W., Symmetry breaking in the self-assembly of partially fluorinated benzene-1,3,5-tricarboxamides. *Angew. Chem. Int. Ed.* **2012**, *51*, 11297–11301.
28. Shen, B.; Pan, C.; Feng, X.; Kim, J.; Sun, M.; Lee, M., Spontaneous chirality induction in the assembly of a single layer 2D network with switchable pores. *Angew. Chem. Int. Ed.* **2023**, *62*, e202300658.
29. Buhse, T.; Cruz, J.-M.; Noble-Terán, M. E.; Hochberg, D.; Ribó, J. M.; Crusats, J.; Micheau, J.-C., Spontaneous deracemizations. *Chem. Rev.* **2021**, *121*, 2147–2229.
30. Roche, C.; Sun, H.-J.; Prendergast, M. E.; Leowanawat, P.; Partridge, B. E.; Heiney, P. A.; Araoka, F.; Graf, R.; Spiess, H. W.; Zeng, X.; Ungar, G.; Percec, V., Homochiral columns constructed by chiral self-sorting during supramolecular helical organization of hat-shaped molecules. *J. Am. Chem. Soc.* **2014**, *136*, 7169–7185.
31. Yashima, E.; Ousaka, N.; Taura, D.; Shimomura, K.; Ikai, T.; Maeda, K., Supramolecular helical systems: helical assemblies of small molecules, foldamers, and polymers with chiral amplification and their functions. *Chem. Rev.* **2016**, *116*, 13752–13990.

32. Son, D.; Kang, J.; Vardoulis, O.; Kim, Y.; Matsuhisa, N.; Oh, J. Y.; To, J. W. F.; Mun, J.; Katsumata, T.; Liu, Y.; McGuire, A. F.; Krason, M.; Molina-Lopez, F.; Ham, J.; Kraft, U.; Lee, Y.; Yun, Y.; Tok, J. B. H.; Bao, Z., An integrated self-healable electronic skin system fabricated via dynamic reconstruction of a nanostructured conducting network. *Nat. Nanotechnol.* **2018**, *13*, 1057–1065.
33. Wu, X.; Zhu, X.; Chong, P.; Liu, J.; Andre, L. N.; Ong, K. S.; Brinson, K.; Mahdi, A. I.; Li, J.; Fenno, L. E.; Wang, H.; Hong, G., Sono-optogenetics facilitated by a circulation-delivered rechargeable light source for minimally invasive optogenetics. *Proc. Natl. Acad. Sci. U. S. A.* **2019**, *116*, 26332–26342.
34. Skylar-Scott, M. A.; Mueller, J.; Visser, C. W.; Lewis, J. A., Voxelated soft matter via multimaterial multinozzle 3D printing. *Nature* **2019**, *575*, 330–335.
35. Du, Y.; Jiang, Y.; Sun, T.; Zhao, J.; Huang, B.; Peng, D.; Wang, F., Mechanically excited multicolor luminescence in lanthanide ions. *Adv. Mater.* **2019**, *31*, 1807062.
36. Xie, Y.; Li, Z., Triboluminescence: recalling interest and new aspects. *Chem* **2018**, *4*, 943–971.
37. Chen, B.; Zhang, X.; Wang, F., Expanding the toolbox of inorganic mechanoluminescence materials. *Acc. Mater. Res.* **2021**, *2*, 364–373.
38. Wang, H.; Wang, W.; Jin, W. J., σ-Hole bond vs π-hole bond: a comparison based on halogen bond. *Chem. Rev.* **2016**, *116*, 5072–5104.
39. Desiraju, G.; Steiner, T., The weak hydrogen bond: In structural chemistry and biology. Oxford University Press: 2001.
40. Cannizzaro, C. E.; Houk, K. N., Magnitudes and chemical consequences of $R_3N^+$–C–H···O=C hydrogen bonding. *J. Am. Chem. Soc.* **2002**, *124*, 7163–7169.
41. Schwierz, M.; Gorls, H.; Imhof, W., Crystal structure of 1-(piperidin-1-yl)butane-1,3-dione. *Acta Crystallogr., Sect. E: Crystallogr. Commun.* **2014**, *70*, o1297.
42. Desiraju, G. R.; Ho, P. S.; Kloo, L.; Legon, A. C.; Marquardt, R.; Metrangolo, P.; Politzer, P.; Resnati, G.; Rissanen, K., Definition of the halogen bond (IUPAC recommendations 2013). *Pure Appl. Chem.* **2013**, *85*, 1711–1713.
43. Bacon, F., The advancement of learning P.F. Collier & Son: New York, 1605; p 208–209.
44. Hardy, G. E.; Kaska, W. C.; Chandra, B. P.; Zink, J. I., Triboluminescence-structure relationships in polymorphs of hexaphenylcarbodiphosphorane and anthranilic acid, molecular crystals, and salts. *J. Am. Chem. Soc.* **1981**, *103*, 1074–1079.
45. Sweeting, L. M.; Rheingold, A. L., Crystal disorder and triboluminescence: triethylammonium tetrakis(dibenzoylmethanato)europate. *J. Am. Chem. Soc.* **1987**, *109*, 2652–2658.
46. Li, Q.; Li, Z., Molecular packing: Another key point for the performance of organic and polymeric optoelectronic materials. *Acc. Chem. Res.* **2020**, *53*, 962–973.
47. Tu, Y.; Zhao, Z.; Lam, J. W. Y.; Tang, B. Z., Aggregate science: much to explore in the meso world. *Matter* **2021**, *4*, 338–349.
48. Arivazhagan, C.; Maity, A.; Bakthavachalam, K.; Jana, A.; Panigrahi, S. K.; Suresh, E.; Das, A.; Ghosh, S., Phenothiazinyl boranes: a new class of aie luminogens with mega stokes shift, mechanochromism, and mechanoluminescence. *Chem. - Eur. J.* **2017**, *23*, 7046–7051.
49. Wang, J.; Chai, Z.; Wang, J.; Wang, C.; Han, M.; Liao, Q.; Huang, A.; Lin, P.; Li, C.; Li, Q.; Li, Z., Mechanoluminescence or room-temperature phosphorescence: molecular packing-dependent emission response. *Angew. Chem. Int. Ed.* **2019**, *58*, 17297–17302.
50. Hocking, M. B.; VandervoortMaarschalk, F. W.; McKiernan, J.; Zink, J. I., Acetone-induced triboluminescence of triphenylphosphine. *J. Lumin.* **1992**, *51*, 323–334.
51. Walton, A. J., Triboluminescence. *Adv. Phys.* **1977**, *26*, 887–948.
52. Eddingsaas, N. C.; Suslick, K. S., Light from sonication of crystal slurries. *Nature* **2006**, *444*, 163–163.